

## **Supporting information of “Catalytic Hydrogenation of N-4-nitrophenyl Nicotinamide in a Micro-Packed Bed Reactor”**

Supporting information includes the following sections:

S1. Synthesis of N-(4-nitrophenyl) nicotinamide

S2. Catalyst characterization

S3. Mass Transfer Studies

S4. Residence time distribution (RTD) studies

S5. Intermediate characterization

S6. Catalyst stability/regeneration

S7. Flow Regimes

S8. Model Derivation

S9. Solvent Screening

Supporting references

## S1. Synthesis of N-(4-nitrophenyl) nicotinamide

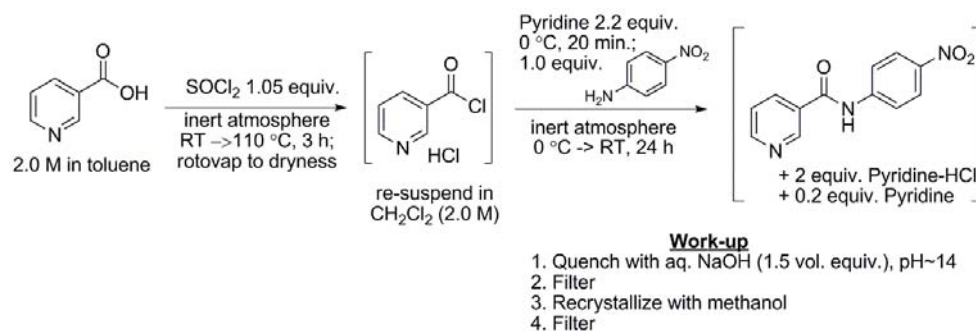


Figure S- 1 . Scheme of synthesis of N-(4-nitrophenyl) nicotinamide

As shown in the scheme of Figure S- 1, N-(4-nitrophenyl) nicotinamide was synthesized in two steps, according to the method reported by Gennäs GB<sup>1</sup>. The brief description of the synthesis steps are shown in below.

In the first step, thionyl chloride (50.0 g, mol, 1.05 equiv.) was added to a 1 L round bottom flask containing a solution of nicotinic acid (50.0 g, 0.x mol) in toluene (325 ml) at 20 °C under a blanket of nitrogen. Upon addition, the flask was fitted with a condenser and heated to reflux for 2-3 hr. After cooling to room temperature, toluene and any remaining thionyl chloride was distilled in vacuo.

In the second step, the resulting crude nicotinoyl chloride HCl salt was resuspended in dichloromethane (325 ml) and cooled to 0 °C under an inert atmosphere. Pyridine was added (72 ml, 2.2 equiv.) and allowed to stir for 20 min, whereupon 4-nitroaniline (56.0 g, 1.0 equiv.) was added. The stirred mixture (500-700 rpm) was allowed to warm to room temperature with stirring for 24 hrs.

Finally, the reaction was quenched and basified to pH = 14 with an aqueous sodium hydroxide solution (4.0 M, 2.2 equiv.). The resulting slurry was filtered. The precipitate was recrystallized in methanol and filtered, producing the product in 90% yield, which was higher than 33% reported previously<sup>1</sup>. The synthesized N-(4-nitrophenyl) nicotinamide was confirmed by H-NMR and LC-MS.

## Section S2. Catalyst characterization

### 2.1. Transmission electron microscopy (TEM) analysis

The morphological analysis was carried out using transmission electron microscopy (TEM) on a JEOL 2010 Advanced High Performance TEM (CMSE at MIT). The fresh Pd/Silica catalyst and deactivated catalyst microparticles were ground by mortar and pestle into fine powders. About 1 mg of fine catalyst powders were added into 2 ml methanol solution to make suspension, 20 µL of which were placed on a hollow copper grid coated with a carbon film (FCF300-CU-50, Electron Microscopy Sciences, PA, USA).

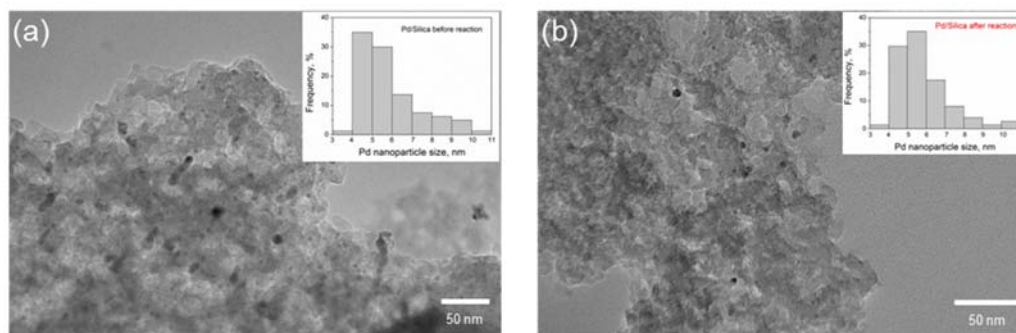


Figure S- 2. TEM images of (a) Fresh Pd/Silica catalyst and (b) Pd/Silica after reaction. Insets are histogram of the Pd nanoparticle sizes based on 100 particles.

The TEM images of fresh Pd/Silica catalyst and deactivated catalyst are shown in Figure S- 2(a) and (b), respectively. The Pd nanoparticles are well-dispersed throughout the silica supports. The insets are histogram of the Pd nanoparticle sizes based on 100 particles, which reflects size distribution between 3–11 nm with average diameter of around 6 nm. 92% of the Pd particles in the size range of 4–9 nm. Especially, the Pd particles from deactivated catalyst show no apparent increase in particle size and broader size distribution. Therefore, we conclude that the deactivation of catalyst during the reaction is not due to the agglomeration of the Pd nanoparticles.

## 2.2. BET surface area and pore size distribution

The specific surface area, pore size distribution studies of the Pd-Silica catalysts was measured using N<sub>2</sub> adsorption isotherms at 77.35 K by the multipoint BET method using Autosorb-iQ (Quantachrome Instruments).

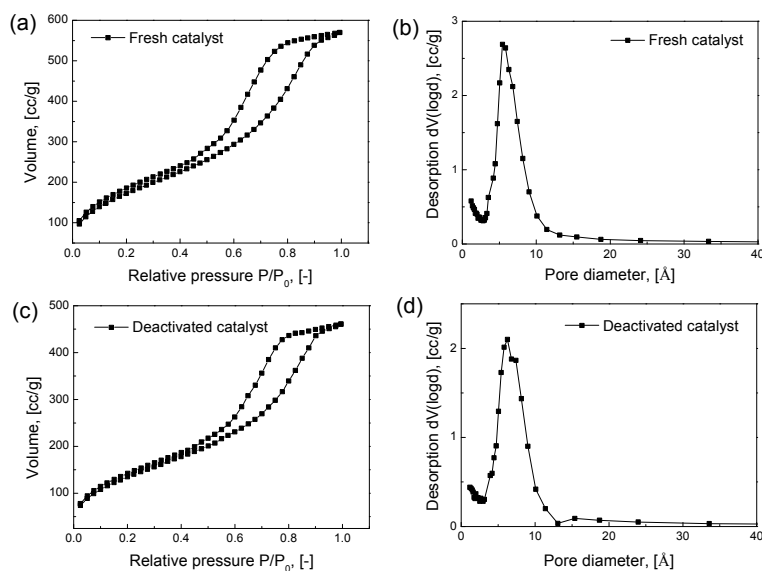


Figure S- 3. BET surface area measurement. Adsorption isotherm of (a) Fresh Pd/Silica catalyst and (c) Deactivated catalyst. BJH desorption pore size distribution of (b) Fresh Pd/Silica catalyst and (d) Deactivated catalyst.

As shown in Figure S- 3(a), the N<sub>2</sub> adsorption–desorption isotherm of the Pd/Silica catalyst shows a typical type IV isotherms with hysteresis loops caused by capillary condensation in mesopores, suggesting that the Pd/Silica catalyst has mesoporous structure. The BJH desorption pore-size distribution curve (Figure S- 3 (b)) shows a sharp peak in the mesopore region and the mean pore diameter is 5.4 nm. The calculated BET surface area is 639 m<sup>2</sup>/g and catalyst pore volume is 0.88 ml/g, shown in Table 1. Similarly, BET measurement was carried out for the deactivated catalyst sample. The isotherm curves and pore size distribution is shown in Figure S- 3 (c) and (d). The measured BET surface area and catalyst pore volume are 505 m<sup>2</sup>/g and 0.706 cc/g, respectively. Around 20% decrease in BET surface area and pore volume was observed, which indicating some coking issues involved during the hydrogenation reaction.<sup>2-4</sup>

## 2.3. CO Chemisorption

The active surface area of Pd was measured by CO chemisorption, which were carried out on an Autosorb-iQ (Quantachrome Instruments). The treatment follows the protocol reported by Losey et al.<sup>5</sup> In detail, the samples (~ 0.5 g) were degassed at 110 °C for 4 h. Next, He pretreatment at 100°C for 30 min was submitted. The catalysts were then reduced under hydrogen for 2 h at 100°C. After the H<sub>2</sub> evaluation and cool-down to room temperature, CO was swept onto the samples. The Pd surface area and metal dispersion were calculated by considering a surface Pd:CO stoichiometry equal to 1.

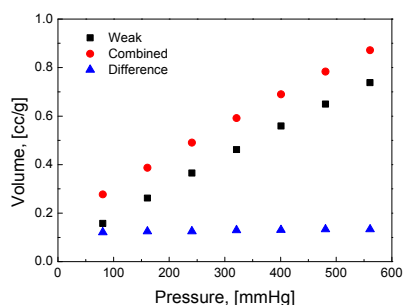


Figure S- 4. Chemisorption analysis of fresh Pd/Silica catalyst.

Figure S- 4 shows the weak (black dotted curve) and combined (red dotted curve) adsorption of CO to the catalyst surface, from which the active Pd surface area was determined to be 0.254 m<sup>2</sup>/g-catalyst. The catalyst after reaction shows Pd surface area of 0.217 m<sup>2</sup>/g-catalyst, which is 14.5% decrease of the fresh catalyst. The TEM images (Figure S- 2) show that there is no Pd agglomeration over reaction, so the decrease of Pd surface area is likely due to the blocking of exposed Pd active sites by deposited cokes.

## Section S3. Mass Transfer Studies

### 3.1. Internal mass transfer

As Pd/Silica catalyst is mesoporous material, the pore limitation is a concern. In order to determine the significance of the internal mass transfer, the Weisz modulus  $M_w$  was calculated by using Equation (S1) and the effective diffusion coefficient  $D_{eff}$  was calculated by Equation (S2).

$$M_w = \eta\phi^2 = \frac{-k'''L^2}{D_{eff}} \quad \text{Eqn. (S1)}$$

$$D_{eff} = D_m \frac{\text{porosity}}{\text{tortuosity}} \quad \text{Eqn. (S2)}$$

Definitions and values supporting this calculation are summarized Table S- 1.

Table S- 1. Definition of parameters for the Weisz modulus calculation

Parameter	Definition	Value	Unit
$R$	Average radius of catalyst particle	90.5	$\mu\text{m}$
$L$	Characteristic length of catalyst particles ( $L=R/3$ for sphere)	30.2	$\mu\text{m}$
$k'''$	Apparent reaction rate constant	0.148	$\text{m}^3 \text{ liquid}/(\text{m}^3 \text{ solid}\cdot\text{s})$
$\phi$	Thiele Modulus $\phi = L \sqrt{\frac{k'''}{D_{eff}}}$	-	-
$D_m$	Molecular diffusivity $D_m = 7.4 \times 10^{-8} \left[ \frac{(\rho M_2)^{0.5} T}{\mu_1 V_1^{0.6}} \right]$ (Wilke-Chang correlation <sup>2</sup> )	7.99 $\times 10^{-9}$ for H <sub>2</sub> 1.45 $\times 10^{-9}$ for N-(4-nitrophenyl)-nicotinamide	$\text{m}^2/\text{s}$
$\varphi$	“association parameter” for the solvent	1.0	
$M_2$	Molecular weight of solvent	DMAC: 87.12 g/mol	
$T$	Temperature	373.15	K
$\mu_2$	Viscosity of solvent	DMAC at 373.15K: 0.653	cp
$V_1$	Molar volume of solute at its normal boiling point (Le Bas method) <sup>3</sup>	14.3 for H <sub>2</sub> 246.3 for N-(4-nitrophenyl)-nicotinamide	$\text{cm}^3/\text{g mole}$
$D_{eff}$	Effective diffusivity $D_{eff} = D_m \frac{\text{porosity}}{\text{tortuosity}}$ (porosity = 0.365, tortuosity $\sim$ 2.7)	1.08 $\times 10^{-9}$ for H <sub>2</sub> 1.96 $\times 10^{-10}$ for N-4-nitrophenyl-nicotinamide	$\text{m}^2/\text{s}$
$M_W$	Weisz Modulus $M_W = \eta \phi^2 = \frac{-r''' L^2}{C_A D_{eff}}$	0.125 for H <sub>2</sub> 0.687 for N-4-nitrophenyl-nicotinamide	-

### 3.2. External mass transfer

In this study, 3 mol/L of alfa-methylstyrene in DMAC solution and pure H<sub>2</sub> gas was concurrently up-flowing into the packed-bed reactor under operating flow rate conditions shown in Table 2 of the text. Alfa-methylstyrene hydrogenation was found to be zero order with respect to alfa-methylstyrene if its concentration is above 10% w/w<sup>6, 7</sup>, and first order to alfa-methylstyrene. Therefore, the observed rate expression is shown in Eq. S3.

Experimental rate constant,  $k_{obs}$ , was determined by fitting the observed rate,

$$r_{obs.} = -\frac{d[\text{AMS}]}{dt} = k_{obs.} [\text{H}_2]^* \frac{\xi_{[\text{H}_2]}}{-\ln(1-\xi_{[\text{H}_2]})} \quad (\text{Eq. S3})$$

where  $[\text{H}_2]^*$  is the saturated concentration of H<sub>2</sub> in the DMAC,  $\xi_{[\text{H}_2]} = (P_{\text{H}_2, in} - P_{\text{H}_2, out})/P_{\text{H}_2, in}$  is the conversion of hydrogen per pass based on the system pressure.<sup>4</sup>  $k_{obs}$  is the apparent reaction rate constant.

According to Losey et al.,<sup>5</sup>  $k_{obs}$  corresponds with overall mass transfer resistance consists of diffusion of the species inside the porous catalysts  $\eta$  and an external mass transfer resistance between gas, liquid and solid phase  $k_{GLS} a_{GLS}$ .

$$\frac{1}{k_{obs}} = \frac{1}{k_{GLS} a_{GLS}} + \frac{1}{\eta k_{intrinsic}} \quad (\text{Eq. S4})$$

In Section 2.1 of this supporting information, we calculated the  $M_w$  number and demonstrated negligible effect of pore diffusion limitation, i.e.  $\eta \approx 1$ .

At 100 °C, the reaction is dominated by mass transfer limitation (i.e.  $\eta^{k_{intrinsic}} \gg k_{GLS}a_{GLS}$ ), thus apparent rate constant is equal to the overall mass transfer rate constant (Eq. S5).<sup>4</sup>

$$k_{obs} = k_{GLS}a_{GLS} = k_{GS}a_{GS} + \left( \frac{1}{k_{GL}a_{GL}} + \frac{1}{k_{LS}a_{LS}} \right)^{-1} \quad (\text{Eq. S5})^4$$

In Eq. S5, three different mass transfer steps for the gas-components are identified.  $k_{GS}a_{GS}$  is the  $H_2$  transfer from gas bubble through liquid film directly to catalyst surface,  $k_{GL}a_{GL}$  is the transfer of  $H_2$  from gas phase into liquid phase, and  $k_{LS}a_{LS}$  is the transfer of dissolved  $H_2$  from liquid to the catalyst surface. In this study, we did not isolated each mass transfer steps, instead, the overall mass transfer  $k_{GLS}a_{GLS}$  is calculated by Eqs. S5 and S3. From the measured apparent reaction rate of alfa-methylstyrene, the mass transfer resistance  $k_{GL}a_{GL}$  was determined, as represented in Table 2.

### Section S4. Residence time distribution (RTD) studies

The packed bed reactor used in this study is composed of two sections: a calming chamber and a catalyst fixed bed. Therefore, careful residence time distribution studies are needed to obtain the accurate residence time in the catalyst bed section. RTD experiments for both reactor (2 cm calming chamber plus 6 cm catalyst bed) and a bypass (2 cm calming chamber packed with only inert glass beads) were carried out. The raw data are shown in Figure S- 5(a)-(d). We assumed “open-open” boundary condition (Eq. S6)<sup>8, 9</sup> for our reactor system first to generate a predicted RTD for the catalytic bed, which was convoluted with the experimental bypass RTD data to generate a reconvoluted curve for the combined system. If the physics within the catalytic bed (i.e. dispersion, and mean residence time), were captured correctly, this new set of reconvoluted RTD data will match with the experimental RTD. A least square curve fit was applied in Matlab to obtain optimized mean residence time  $\tau$  and  $D/uL$  by minimizing the difference between reconvoluted RTD and measured RTD. In addition to the fit value (Figure S- 5 (e)), the mean residence time,  $\tau$  was calculated by Eqs. S7 and S8.

$$C(\theta) = \sqrt{\frac{uL}{4\pi\theta D}} \exp\left(-\frac{uL}{4\pi D}(1 - \theta)^2\right) \quad (\text{Eq. S6})$$

$$E(t) = \frac{C(t)}{\int_0^\infty C(t) dt} \quad (\text{Eq. S7})$$

$$\bar{\tau} = \int_0^\infty t \times E(t) dt \quad (\text{Eq. S8})$$

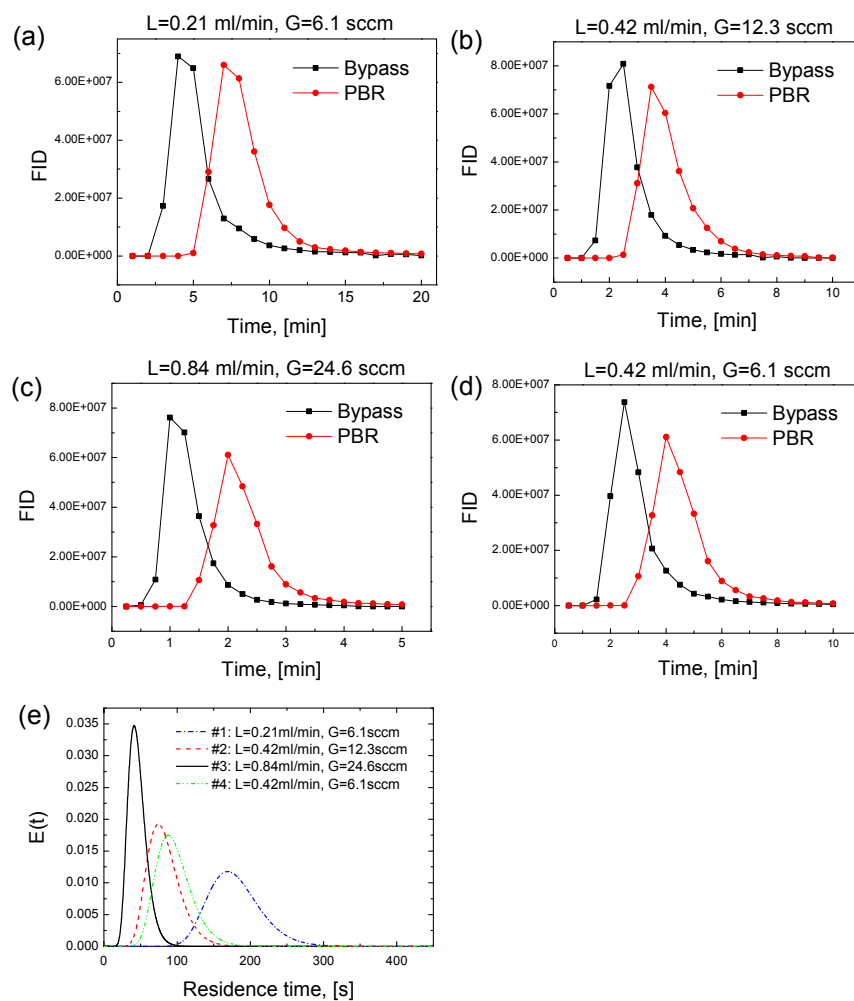


Figure S- 5. RTD studies. (a)-(d) Raw data of residence time distribution of liquid tracer toluene in both PBR and bypass reactor. (e) Simulated results for four flow conditions based on open-open boundary condition assumption.

## Section S5. Intermediate characterization

### 5.1. $^1\text{H}$ and $^{13}\text{C}$ NMR spectra

The collected reaction solution was analyzed by analytical TLC and further separated by preparative TLC plate (Sigma-Aldrich, Z513032) with mixed solvent (dimethyl chloride (DCM)/methanol (MeOH)=4:1). The purified dimer intermediate ((E)-2-(3-(nicotinamido)phenyl)-1-(4-(nicotinamido)phenyl)diazene 1-oxide, compound D in Scheme 2) was dissolved in deuterated DMSO and analyzed by  $^1\text{H}$  and  $^{13}\text{C}$  NMR, as shown in Figure S- 6 and Figure S- 7.

$^1\text{H}$  and  $^{13}\text{C}$  NMR spectra were recorded on a Bruker 400 MHz (Department of Chemistry Institute Facility (DCIF)) in MIT in DMSO- $d_6$  at ambient temperature unless otherwise indicated. Chemical shifts are reported in  $\delta$  (ppm downfield from tetramethylsilane) and referenced to residual undeuterated solvents (2.50 for  $^1\text{H}$  NMR and 39.52 for  $^{13}\text{C}$  NMR). Coupling constants are reported in Hz with multiplicities denoted as s (singlet), d (doublet), m (multiplet), app (apparent).

$^1\text{H}$  NMR (600 MHz, DMSO- $d_6$ )  $\delta$  10.91 (s, 1H), 10.82 (s, 1H), 9.17-9.12 (m, 2H), 8.82-8.76 (m, 2H), 8.39-8.32 (m, 2H), 8.30 (app d, 2H,  $J = 8.4$ ), 8.26 (app d, 2H,  $J = 8.4$ ), 8.05 (app d, 2H,  $J = 8.8$ ), 7.99 (app d, 2H,  $J = 8.8$ ),

7.63-7.57 (m, 2H);  $^{13}\text{C}$  NMR (150 MHz,  $\text{DMSO}-d_6$ )  $\delta$  164.6, 164.4, 152.4, 152.3, 148.84, 148.79, 142.9, 142.2, 140.1, 139.4, 135.7, 135.6, 130.4, 130.2, 126.3, 123.54, 123.53, 122.7, 120.03, 119.98. HRMS (ESI) calcd for  $\text{C}_{24}\text{H}_{17}\text{N}_6\text{O}_3$  ( $\text{M}-\text{H}$ ) $^-$  437.1368, found 437.1379.

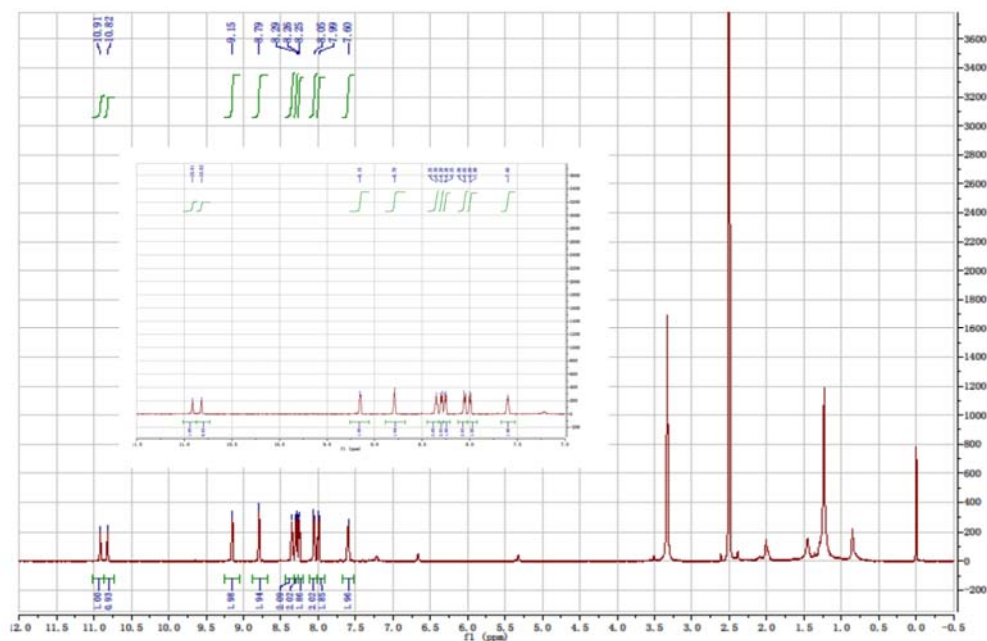


Figure S- 6.  $^1\text{H}$  NMR of compound **D**

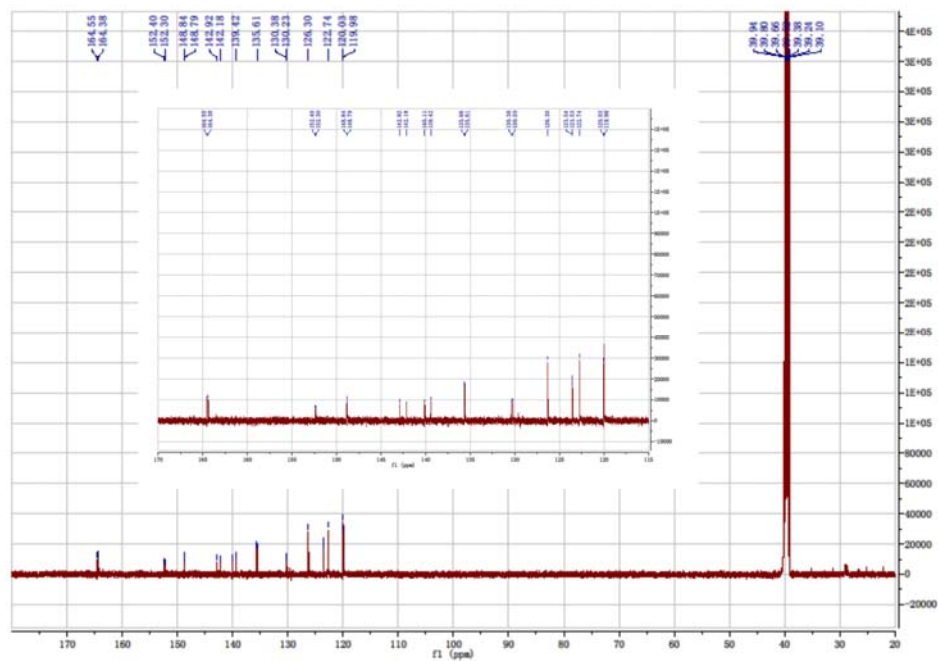


Figure S- 7.  $^{13}\text{C}$  NMR of compound **D**

## 5.2. High-resolution mass spectra

The exact molecular mass of intermediate compound D was determined by high-resolution MS installed with ionization source of electrospray (ESI) in DCIF of MIT. The measured exact mass to four decimal places is 437.1379, which is close to the theoretical mass of 437.1368.

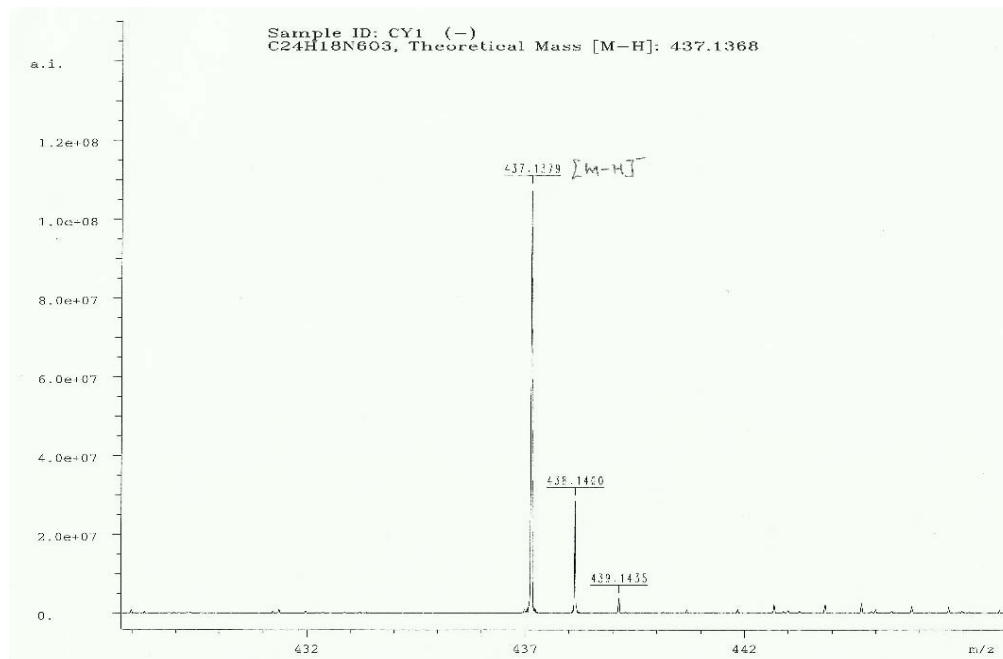


Figure S- 8. High-resolution MS of compound D

## Section S6. Catalyst stability/regeneration

The catalyst life is extremely important. The replacement of a fixed catalyst bed should be avoided, as the process is troublesome and involves a loss of possible production time. Therefore, in-situ catalyst regeneration is preferred. As shown in Figure S- 9, under non-optimized flow condition at 80 °C, the conversion and selectivity show about 10% decrease over 3 hours continuous operation. The catalyst was prone to deactivation when intermediates are accumulated. By polymerization and condensation reactions, tar and coke were formed. Therefore, we follow the regeneration procedure reported by Westerterp et al<sup>6,10</sup>. Low flow rate air was added into the packed bed reactor system for 2 hours at 130 °C, at which temperature coke and coke can be burned off in air. After this, flown into the packed bed reactor at 130 °C for another 2 hours by hydrogen to reduce the Pd into metallic state.

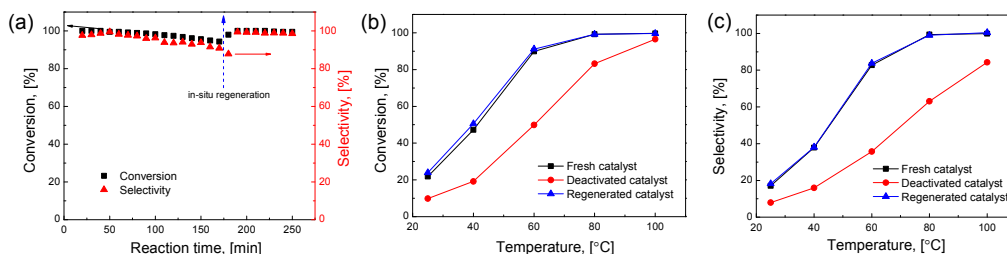


Figure S- 9. In-situ generation of Pd/Silica catalysts. (a) Continuous hydrogenation in the packed bed reactor. Flow condition:  $u_L=0.4\text{ml/min}$ ,  $u_G=12\text{sccm}$ ,  $T=80^\circ\text{C}$ . Comparison of conversion (b) and selectivity (c) for fresh, deactivated and regenerated catalysts under various temperature.

## Section S7. Flow Regimes

As total flow rate (gas + liquid) is increased at constant gas-to-liquid flow ratios and constant pressure, the pressure drop across the packed column is observed to increase, as expected porous media (Figure S- 10). However, pressure pulsation/instabilities are observed with greater deviation at low flows (error bars, Figure S- 10). This finding, in conjunction with the variance in residence time distributions (Table 3 of main text) and known complexity of micro-packed beds<sup>7</sup> leads to the conclusion that multiphase hydrodynamics are expected to be variable in the current study.

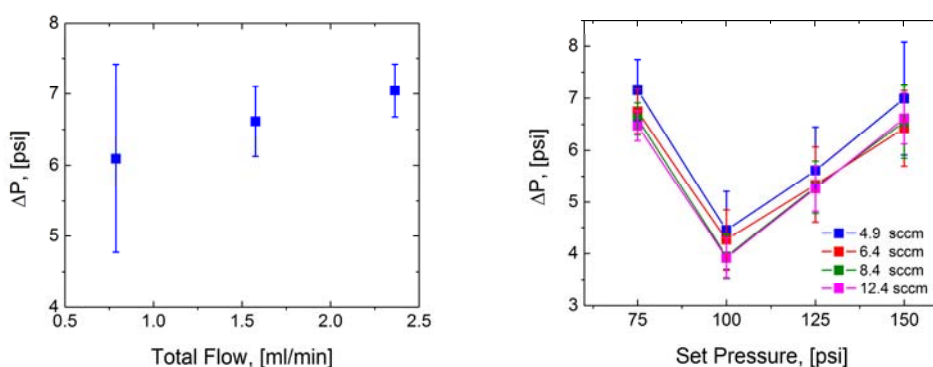


Figure S- 10. Flow Stabilization. (a) Flow rate is uniformly increased with constant gas-to-liquid flow rate,  $\alpha = 2.9$  at 150 psi. Signal to noise (error bars = 1 standard deviation), decreases with increases in flow, indicating a more stabilized flow with less pulsation at higher flow rates. (b) Liquid Flow = 0.4 ml/min. As set pressure is increased, pressure drop generally increases ( $P \geq 100$  psi), and slight increases to standard deviation is observed. Variability in stable flow regimes contributes to discontinuity of pressure drop profile.

## Section S8. Model Derivation

A simplified kinetic model (inset Figure 4 of the main text) describing the reactant (A), azo intermediate (D) and primary amine product (P) was developed and applied to a dispersion-reaction packed bed reactor model.

$$\frac{\partial C_i}{\partial t} + u \nabla C_i = \mathfrak{D} \nabla^2 C_i + R_{V,i}, \quad i = [A, D, P] \quad \text{Eq. S9}$$

Where  $C_i$  is the concentration of species  $i$ ;  $t$  is the reaction time,  $u$  is the average flow velocity,  $\mathfrak{D}$  is the dispersion coefficient in the bed, and  $R_{V,i}$  is the reaction rate. Neglecting radial gradients, the 1D system steady state mass balance reduces to,

$$u_z \frac{dC_i}{dz} = \mathfrak{D} \frac{d^2 C_i}{dz^2} + R_{V,i} \quad \text{Eq. S10}$$

Made dimensionless by defining  $\theta_i = C_i/C_{A0}$ , where  $C_{A0}$  is the initial concentration of  $A$ ,  $\eta = z/L$  is the normalized reactor length and  $Bo = u_z L/\mathfrak{D}$ . The second Damkholer number for the  $j^{th}$  first order reaction representing the ratio of reaction rate to axial dispersion is defined as  $Da_j = k_j L^2/\mathfrak{D}$ . The corresponding system of equations become,

$$0 = \frac{d^2 \theta_i}{d\eta^2} - Bo \frac{d\theta_i}{d\eta} + \frac{L^2}{\mathfrak{D} C_{A0}} R_{V,i} \quad \text{Eq. S11}$$

$$\frac{L^2}{\mathfrak{D} C_{A0}} R_{V,i} = \begin{cases} -(Da_1 + Da_2)\theta_A, & i = A \\ 2Da_2\theta_A - Da_3\theta_D, & i = D \\ Da_1\theta_A + 2Da_3\theta_D, & i = P \end{cases}$$

As with the hydrodynamic model from the RTD study, the two boundary conditions are taken to be the standard 'open-open' conditions whereby dispersion in the inlet (calming chamber/catalytic bed interface) is considered, and continuity across the outlet:

$$\left. \frac{d\theta}{d\eta} \right|_{\eta=0} = \left. \frac{d\theta}{d\eta} \right|_{\eta=1} = 0, \quad \theta_{i,0} = \begin{cases} 1 & i = A \\ 0 & i \neq A \end{cases} \quad \text{Eq. S12}$$

The second order nonlinear system of ODE's was solved using the Matlab 2016a numerical integration function `bvp4c`. To fit lumped rate constants ( $k_1$ ,  $k_2$ , and  $k_3$ ), a least squares nonlinear regression (`lsqnonlin`) was performed to minimize the unweighted error between model predictions at the effluent ( $\eta = 1$ ) and the measured experimental values at all flow rates. To ensure the robustness of the fit, a global minimization was performed using the Matlab function `multistart` across five orders of magnitude in initial guesses and fifty distinct starting points. The resultant fits are shown in Figure 4.

The reaction flux for each chemical reaction ( $j$ ), can be quantitatively assessed by calculating the respective fluxes at each residence time.

$$R_{V,j} = \begin{cases} k_1 C_A = k_1 C_{A0} \theta_A, & j = 1 \\ k_2 C_A = k_2 C_{A0} \theta_A, & j = 2 \\ k_3 C_D = k_3 C_{A0} \theta_D, & j = 3 \end{cases} \quad \text{Eq. S13}$$

The model is further simplified for reaction optimization to account for only the rate determining step. Starting with Eq. 3-4, the following assumptions are applied:

- (1) Overall reaction rate is approximated by the first order consumption of the reactant species.
- (2) Dispersion is low (i.e.  $Bo \gg 1$ , as measured in Table 3).
- (3) Constant holdup throughout the reactor with uniform catalyst packing ( $\rho_{cat}$ ).

Based on the above assumptions, the standard packed bed reactor model<sup>11</sup> was applied to elucidate intrinsic rates from steady state reactor operation with differential conversion ( $dX_A$ ) measured at several weighted residence times across a differential segment ( $dw$ ),

$$F_{A0} dX_A = V_{A0} C_{A0} dX_A = -r'_A dw \quad \text{Eq. S14}$$

where  $r'_A$  is the reaction rate per unit mass of catalyst. To relate the differential species balance to the effluent concentrations observed experimentally, Eq. 6 was integrated over the active bed based with the first order kinetics assumption ( $r'_A = k'C_A$ ) to obtain,

$$-\ln(1-X_{Af}) = \frac{w k' C_{A0}}{F_{A0}} = k' \frac{w}{V_{A0}} \quad \text{Eq. S15}$$

## Section S9. Solvent Screening

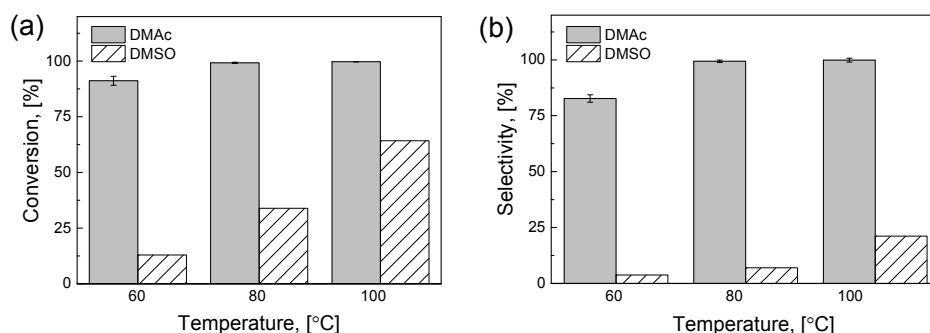


Figure S- 11. The comparison of solvents dimethyl sulfoxide (DMSO) and DMAc on the catalytic performance. (a) Conversion comparison. (b) Selectivity comparison.

Catalytic hydrogenation reactions were carried out with the same initial concentration of starting material but in different solvent DMSO under the same flow conditions. As shown in Figure S- 11, higher apparent conversion and selectivity towards the target product were achieved in DMAc solvent when compared to DMSO. At 100 °C, the conversion of starting material with DMSO as solvent is only 64%, and the selectivity is 21%, showing inhibited catalytic performance in comparison with reaction in DMAc solvent. The exploration of the underlying mechanism is still unknown. A possible explanation may be that the sulfide atom from DMSO may poison the Pd catalyst.<sup>8,9</sup> Indeed, we found that the deactivated Pd/Silica catalyst used in DMSO solvent failed to be regenerated with the same regeneration protocol we mentioned in Section S3 in this supporting information.

### Supporting References:

1. G. B. af Gennas, L. Mologni, S. Ahmed, M. Rajaratnam, O. Marin, N. Lindholm, M. Viltadi, C. Gambacorti-Passerini, L. Scapozza and J. Yli-Kauhaluoma, *ChemMedChem*, 2011, **6**, 1680-1692.
2. R. C. Reid and T. K. Sherwood, *Properties of Gases and Liquids* McGraw-Hill Inc., 1966.
3. B. E. Poling, J. M. Prausnitz and J. P. O'Connell, *The properties of gases and liquids*, McGraw-Hill, 2001.
4. M. T. Kreutzer, P. Du, J. J. Heiszwolf, F. Kapteijn and J. A. Moulijn, *Chemical Engineering Science*, 2001, **56**, 6015-6023.
5. M. W. Losey, M. A. Schmidt and K. F. Jensen, *Industrial & Engineering Chemistry Research*, 2001, **40**, 2555-2562.
6. K. B. van Gelder, J. K. Damhof, P. J. Kroijenga and K. R. Westerterp, *Chemical Engineering Science*, 1990, **45**, 3159-3170.
7. J. Zhang, A. R. Teixeira, L. T. Kögl, L. Yang and K. F. Jensen, *AIChE Journal*, DOI: 10.1002/aic.15807, n/a-n/a.

8. P. Albers, J. Pietsch and S. F. Parker, *Journal of Molecular Catalysis A: Chemical*, 2001, **173**, 275-286.
9. P. A. Gravil and H. Toulhoat, *Surface Science*, 1999, **430**, 176-191.
10. K. R. Westerterp, E. J. Molga and K. B. van Gelder, *Chemical Engineering and Processing: Process Intensification*, 1997, **36**, 17-27.
11. H. S. Fogler, *Elements of Chemical Reaction Engineering*, Pearson Education, 2016.